Nanomaterials/Polymer-Integrated Flexible Sensors: A Full-Laser-Processing Approach for Real-Time Analyte Monitoring

Maxim Fatkullin, Elizaveta Dogadina, Il'ya Bril', Alexey Ivanov, Aleksandar Matkovic, Raul D. Rodriguez, and Evgeniya Sheremet

***Abstract*—In this study, we develop fully laser-made electrochemical "drop sensors," including all three electrodes as in conventional screen-printed electrodes. Our approach is based on the laser processing of graphene oxide (GO) and silver nanoparticle films on a polyethylene terephthalate (PET) substrate to produce electrically conductive and robust free-form composites. The system contains laser-reduced graphene as working and counter electrodes, while laser-integrated silver serves as the reference electrode. We systematically investigate the structural, electrical, and electrochemical properties of these electrodes, showing that our optimized laser processing allows creating electrodes with a near-record low sheet resistance of 29 ± 2 Ω sq^{-1}. We successfully demonstrated the practical implementation of the sensor for caffeine detection in a 200-μL drop with a sensitivity of 17 ± 3 μA mM^{-1} highlighting its efficiency in a small-volume analysis. Remarkably, this laser processing approach enabled devices that retained their sensing performance even after undergoing 1000 bending cycles. These findings have significant implications for the development of flexible, sensitive, and robust devices in various applications, ranging from healthcare monitoring to environmental sensing, highlighting the transformative potential of laser-based sensor fabrication technology.**

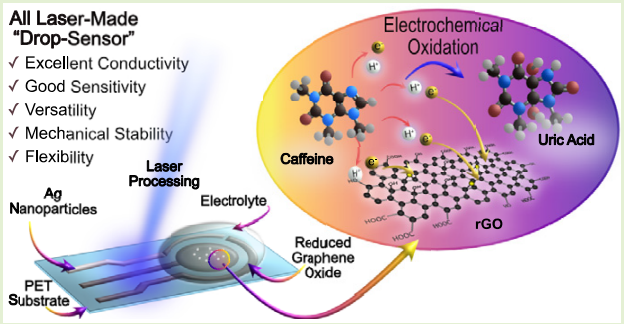

***Index Terms*— Electrochemical sensor, graphene/polymer composite, laser processing, reduced graphene oxide (GO).**

I. Introduction

ELECTROCHEMICAL sensors have experienced a profound transformation in recent years [1], driven by the ever-growing search for innovative materials capable of increasing the performance and versatility of sensing devices [2], [3]. Among these materials, reduced graphene oxide (rGO) has emerged as a promising option, due to its high electrical conductivity [4], remarkable surface area [5], and robust electrochemical stability [6], [7], [8].

The superiority of rGO lies in its 2-D carbon lattice, which provides substantial surface area for analyte adsorption and edge-plane-like defective sites, which facilitates rapid electron transfer, enabling fast, sensitive, wide potential window [9], and selective electrochemical response [10]. Due to this, rGO in electrochemical sensors conventionally serves as the working electrode allowing it to mediate electrochemical reactions of the target analyte. Target-rGO electrode interactions include adsorption [11], redox reactions [12], or other electrochemical processes, depending on the specific analyte [13].

RGO electrochemical sensors cover a wide range of applications and can detect such analytes as dopamine, ascorbic acid [14], glucose [6], [15], caffeine [16], acetaminophen [17], heavy metals [18], and nitrite [19]. Moreover, electrochemical sensing has a critical application with far-reaching implications in healthcare and beyond [20]. All the aforementioned molecules in one or another way influence human well-being. In particular, caffeine is one of the most widely spread legal stimulants (aka soft drugs), which consistently over-consuming could affect human mental health and

Manuscript received 7 December 2023; revised 10 February 2024; accepted 11 February 2024. Date of publication 5 March 2024; date of current version 1 May 2024. This work was supported by the Russian Science Foundation under Grant № 22-12-20027 and the funding from Tomsk region administration. The work of Aleksandar Matkovic was supported by the Austrian Science Fund (FWF) under Grant I4323-N36 and Grant Y1298-N. The associate editor coordinating the review of this article and approving it for publication was Prof. Yu-Cheng Lin. *(Corresponding author: Raul D. Rodriguez.)*

Maxim Fatkullin, Elizaveta Dogadina, Il'ya Bril', Alexey Ivanov, Raul D. Rodriguez, and Evgeniya Sheremet are with the Research School of Chemical and Biomedical Technologies, Tomsk Polytechnic University, 634050 Tomsk, Russia (e-mail: fatkullin.262@gmail.com; elizavetadogadina@gmail.com; ellaijiah@gmail.com; ivanovaa@tpu.ru; raul@tpu.ru; jane.sheremet@gmail.com).

Aleksandar Matkovic is with the Chair of Physics, Department Physics, Mechanics and Electrical Engineering, Montanuniversität Leoben, 8700 Leoben, Austria (e-mail: aleksandar.matkovic@unileoben.ac.at).

This article has supplementary downloadable material available at https://doi.org/10.1109/JSEN.2024.3371005, provided by the authors.

Digital Object Identifier 10.1109/JSEN.2024.3371005

behavior, bone condition, and lead to the appearance of cardiovascular diseases [21], [22]. That is why sensitive and fast caffeine detectors are being intensively developed.

Among the common rGO production methods, laser processing is particularly advantageous since it allows the efficient and selective creation of low-cost arbitrarily shaped electrodes on various substrates, including thermosensitive polymers, ideal for flexible and wearable devices [23]. Joshi et al. [24] made an electrochemical sensor based on laser-reduced graphene oxide (GO) for H_2O_2 detection. The sensor has a high resistivity of 3×10^{-2} Ω·cm and a record limit of detection (LoD) of 7.15 nM. Singh et al. [25] developed a sensor based on laser-induced reduced GO on paper for the detection of dopamine, uric, and ascorbic acids with LoD 26–29 μM. Furthermore, rGO is a popular material for caffeine detection due to electrostatic and π–π interactions, but most studies used chemical or electrochemical methods for GO reduction [26].

Here, we develop the topic further by presenting a new concept based on a fully laser-integrated electrochemical sensor on a polyethylene terephthalate (PET) substrate. Our design not only incorporates rGO for working and counter electrodes but also employs laser-integrated silver nanoparticles (AgNPs) as the reference electrode. This innovative sensor design and fabrication enable high sensitivity and a suitable for real application LoD as illustrated by caffeine detection, reaching values of 17 ± 3 μA mM^{-1} and 0.01 mM, respectively. This high sensitivity and sensor design add adaptability and responsiveness, making it valuable in various real-time caffeine monitoring scenarios. Additionally, we show the universality of our fabricated "drop sensors" by performing glucose detection for concentrations within a medically significant range. Crucially, our "drop sensors" also exhibit remarkable flexibility, maintaining consistent sensing performance even after 1000 bending cycles. This feature shows the sensor's potential in wearable and adaptable healthcare monitoring devices.

II. Experimental Section

A. Materials

Materials and reagents used within this work were: the distilled water used in the experiments was obtained using a Millipore Milli-Q system (Merck, Germany). GO aqueous dispersion (Graphenea, Spain), potassium ferricyanide (KhimMedSnab, Russia), phosphate-buffer saline (Uralkhim-invest LLC, Russia), potassium hydroxide (Sigma Aldrich), glucose (SC Flora Kavkaza, Russia), caffeine (Sigma Aldrich), AgNPs (Advanced powder technologies, Russia), sulfuric acid (KhimMedSnab, Russia), boric acid (KhimMedSnab, Russia), acetic acid (KhimMedSnab, Russia), sodium hydroxide (KhimMedSnab, Russia), high-performance liquid chromatography (HPLC)-grade acetonitrile (Panreac), and TFA (Sigma-Aldrich). All the reagents were chemical grade and were used as received without any additional purification.

B. rGO/PET Electrode Fabrication

rGO/PET was fabricated using GO and a PET sheet 0.7 mm thick (SafPlast, Russia). The aqueous dispersion of GO (4 mg/mL) was drop-casted onto a PET sheet with an amount of 90 μL/cm^2 and left to dry in ambient conditions to form a film. The film was then laser processed with a diode pulsed laser (438-nm wavelength, pulse energy ~0.17 J, and pulsewidth ~260 μs). Furthermore, the residues of the film and poorly integrated GO were removed via sonication in distilled water for 1 min.

C. "Drop-Sensor" Fabrication

"Drop sensors" were fabricated through a several-step procedure. First, the rGO working and counter electrode was prepared following the procedure described above, with a predefined SPE electrode geometry pattern. After removing the GO film, the film of AgNPs was made by drop-casting of 1.5-mL AgNPs ethanolic dispersion (100 mg per 1.5 mL; 75 μL/cm^2) and left to dry in ambient conditions. The reference electrode was formed by laser processing of AgNPs film with the same laser but with different parameters (~0.12 J per pulse, ~210 μs). After the laser processing, the residues of the film were removed by sonication in distilled water for 1 min.

D. Four-Point Probe Measurements

Sheet resistance was measured using Potentiostat/Galvanostat P-45X with FRA-24M impedance modulus (Electrochemical instruments, Russia) coupled with MST 4000A microprobe station (MS Tech Korea Company Ltd., South Korea) to position the probes in a square configuration with 400 μm side length. The current of 1 mA was applied along the side of the square and voltage drop was measured along the parallel side. The sheet resistance of the material was calculated using the equation [27]

$$R_{\text{sheet}} = \frac{V \cdot 2\pi}{I \cdot \ln 2} \tag{1}$$

where V (V) is the measured voltage and I (A) is the applied current. To assess the dispersion and statistical significance, the sheet resistance of five samples was measured at three distinct spots on each sample, collecting 1000 data points per spot.

E. SEM and Energy-Dispersive X-Ray Spectroscopy

The scanning electron microscopy (SEM) and the selected-area energy-dispersive X-ray spectroscopy elemental mapping were performed with the Tescan Mira 3LMU and ULTIM MAX 40.

F. X-Ray Photoelectron Spectroscopy

The X-ray photoelectron spectroscopy (XPS) was performed using a Thermo Fisher Scientific XPS NEXSA spectrometer with a monochromatic Al K Alpha X-ray source working at 1486.6 eV. The survey study was made with a pass energy of 200 (eV) and an energy resolution of 1 eV. For the high-resolution spectra, the pass energy was 50 (eV) and the energy resolution was 0.1 (eV) with a spot diameter of 400 μm.

G. Raman Spectroscopy

Raman spectra were recorded using a confocal Raman microscope (NTEGRA Spectra, NT-MDT, Russia) with a

532-nm diode excitation laser. The Mitutoyo objective with 20× magnification was used to focus a laser beam on the sample surface and record spectra with 5-s exposure time and five times accumulation.

H. Electrochemical Characterization

Electrochemical characterization was carried out in the PBS using a three-electrode cell with rGO/PET, platinum, and Ag/AgCl (saturated KCl) as working, counter, and reference electrodes, respectively. Cyclic voltammetry (CV) measurements and electrochemical impedance spectroscopy (EIS) were carried out using Corrtest CS2350M (Corrtest, China). EIS was measured in the frequency range of 0.25 Hz–100 kHz. Electron transfer characteristics were assessed in 5-mM $K_4[Fe(CN)_6]$ solution in 0.1-M KCl as a supporting electrolyte.

I. Electrochemical Sensing

Electrochemical sensing was carried out using Corrtest CS2350M (Corrtest, China) on the fabricated "drop sensors." Caffeine sensing was carried out in a caffeine solution with different concentrations in the self-prepared Brittan–Robinson buffer (pH 2) as a supporting electrolyte. Glucose sensing was performed in the glucose solution in 0.1-M KOH as a supporting electrolyte. All the measurements were carried out using 200 μL of solutions. The LoD for the sensor was mathematically assessed as an intercept of the calibration with the concentration axis (the point where the peak current is equal to zero).

Instant coffee analysis was carried out the following way; 7.2 g of instant coffee was dissolved in 25 mL of distilled water under constant stirring and heating to 110 °C for 5 min. Then, 50 μL of this solution was added to 950 mL of self-prepared Brittan–Robinson buffer (pH 2). After that, electrochemical sensing was performed using 200 μL of sample.

J. High-Performance Liquid Chromatography

HPLC was performed on an HPLC Agilent 1200 system with a diode array detector (1260 DAD VL). Chromatography was carried out using a Zorbax (Agilent Technologies, USA) Eclipse Plus C18 column (4.6 mm · 100 mm, 5 μm) at 30 °C. HPLC mobile phases were prepared using water Type I (Milli-Q IQ 7003, Merck), HPLC-grade acetonitrile, and TFA. Analysis was performed using 0.1% trifluoroacetic acid in water (phase A)–CH_3CN (phase B) as the mobile phase, which was introduced by isocratic elution with ratio A:B = 92:8 for 10 min. The injection volume was 20 μL. UV detection was carried out at 275 nm. Before analysis, every sample was filtered through a 0.45-μm nylon syringe filter. Each sample was analyzed three times.

K. Bending Test

The bending test was performed in a self-made three-point bending setup, where the "drop sensor" was fixed in its ends and the bending piston was applying force to its middle; 1000 cycles at a frequency of 0.56 Hz were conducted.

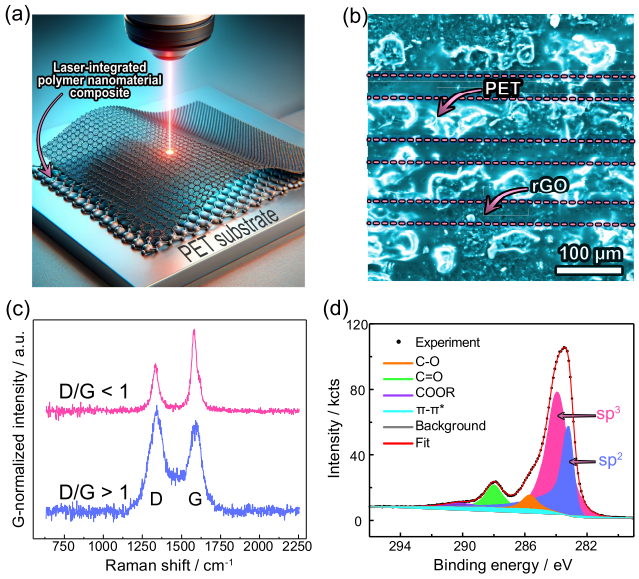

Fig. 1. (a) Schematic illustration of the GO film laser processing on PET. (b) SE SEM image of the rGO/PET surface, where the bright charged areas were identified as PET and rough dark areas as rGO. The pink-highlighted lines are correlated with the scanning direction and line separation. (c) Raman spectra from the two representative regions on the sample, with D/G ratio less and more than 1. (d) C 1s high-resolution XPS spectrum from rGO/PET electrode.

III. Results and Discussion

A. GO/PET Electrode Fabrication

We successfully developed graphene-based flexible composite electrodes through a laser processing method applied to a GO film on a 0.7-mm-thick PET sheet, as illustrated in Fig. 1(a). Based on our previous experience in the integration of nanomaterials into various substrates [28], [29], [30], [31], [32], we used a 436-nm laser diode to induce simultaneous GO reduction and composite formation with PET. First, GO absorbs the light, converting its energy to heat and inducing photochemical reactions. This leads to the removal of oxygen-rich functional groups from the GO, effectively transforming it into reduced GO. This transformation changes the optical properties of the film; as more functional groups are eliminated, rGO's absorption increases. This enhanced absorption promotes photothermal transduction efficiency, eventually raising the temperature to a level that melts the underlying PET. Once PET is in the molten phase, it is expected that rGO flakes could penetrate its structure. After ceasing the laser exposure, the molten PET cools down and resolidifies leading to the formation of a rGO/PET composite. The presence of rGO within the PET matrix provides electrical conductivity to the composite system, significantly reducing the sheet resistance from an initial ∞ Ω sq^{-1} to an impressive 25 ± 2 Ω sq^{-1}.

The composite formation was verified by testing the coating stability via ultrasonication in distilled water, using the sheet resistance as a benchmark. Following a 1-min ultrasonication treatment, the rGO/PET electrodes maintained their electrical properties, with a sheet resistance of ca. 29 ± 2 Ω sq^{-1}, a value nearly identical to the initial state. The small deviation of sheet resistance (∼7%) across the five fabricated electrodes indicates

the high reproducibility of the electrodes. This composite formation was further verified by SEM analysis [Fig. 1(b)], revealing two distinctive regions. The first region, rich in rGO, appears darker in the secondary electrons (SEs) image, indicating the composite's layer presence. The second region, predominantly made out of polymer, is characterized by bright charged spots in the SE image. The emergence of these different regions could be attributed to the power distribution within the laser spot along with other factors, such as convective flow and hydrodynamic effects, which need to be clarified in future works on the rGO/polymer composite formation mechanism.

SEM imaging also revealed a highly rough and inhomogeneous morphology of the rGO/PET electrodes, which is advantageous for electrochemical sensing. Cross section SEM images (Fig. S1) allowed us to estimate the thickness of conductive rGO to be ca. 15–20 μm. Building on these results, Raman spectroscopy offered a further understanding of the rGO/PET electrodes' surface heterogeneity, as illustrated in Fig. 1(c). Although most spectra recorded from the rGO/PET surface exhibited the characteristic D (defect-activated band) and G (sp^2 carbon band) modes typical for carbon allotropes, variations in intensity ratio and other parameters were observed across different areas. Some regions showed highly defective carbon, evidenced by a D/G intensity ratio greater than 1 and broader peak widths, while others displayed graphene-like spectra with a D/G ratio below 1 and sharper G peaks.

Further surface chemical analysis was conducted using XPS. The XPS spectra of the rGO/PET composite showed typical rGO peaks. The C 1 s high-resolution region [Fig. 1(d)] was deconvoluted into several bands: sp^2 and sp^3 hybridized carbon (283.4 and 284.3 eV, respectively), C–O (285.7 eV), C = O (288.3 eV), COOR (290 eV), and π–$\pi*$ satellite (292 eV). The calculated sp^2/sp^3 ratio of 0.88 $\pm$ 0.71 was unexpected since rGO generally exhibits a sp^2/sp^3 ratio greater than 1. This anomaly, along with the high variance, could be attributed to the significant polymer presence on the surface, as evidenced by SEM imaging. The XPS spectra, measured with a 400-μm spot diameter, are notably influenced by PET and the sample's overall inhomogeneity, where some regions of rGO may contain nonlaser-treated material. It is further supported by the PET-specific bands in the XPS C 1s spectra (Fig. S2). Nevertheless, the calculated C/O ratio of 4.42 $\pm$ 0.11 from the survey spectra (Fig. S3) further confirms the successful reduction of GO.

B. Electrochemical Characterization of the rGO/PET Electrode

Aiming at sensing applications, it is essential to thoroughly investigate the electrochemical properties of electrodes, including aspects, such as capacitance, electron transfer dynamics, and charge transfer efficiency.

The first step in our characterization process involved recording cyclic voltammograms from the laser-processed rGO/PET electrode [Fig. 2(a)]. These cyclic voltammetry (CV) curves were obtained using a standard three-electrode cell setup, comprising a Pt wire as the counter electrode,

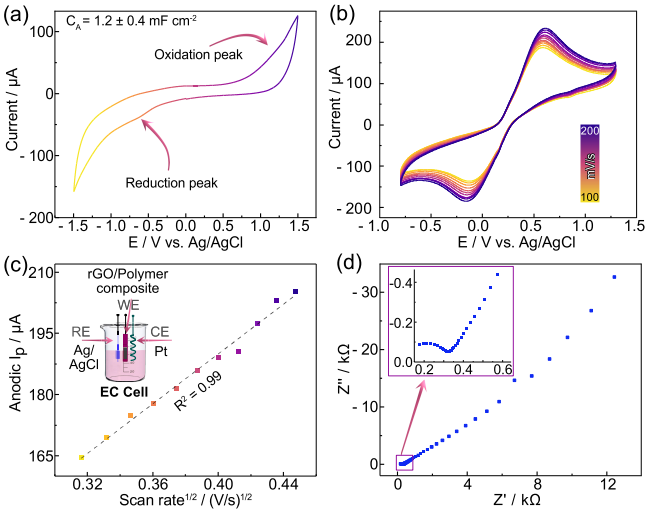

Fig. 2. (a) CV curves from rGO/PET electrode in PBS (pH 2). (b) CV curves from a rGO/PET electrode measured with different scan rates in the presence of 5-mM $K_4[Fe(CN)_6]$ solution in 0.1-M KCl as a supporting electrolyte. (c) Anodic peak current ($K_4[Fe(CN)_6]$ oxidation) versus square root of scan rate and the linear approximation from this (dashed line). (d) Nyquist plot measured on the rGO/PET electrodes. The inset presents a zoom-in to the high-frequency region, which is represented by a semicircle.

Ag/AgCl (saturated KCl) as the reference electrode, and the rGO/PET composite as the working electrode. The experiments were conducted in a phosphate-buffered saline (PBS) with a pH of 6.86. The rGO/PET electrode exhibited primarily capacitive behavior, characterized by a modest oxidation peak at approximately 1 V and a subtle reduction peak around −0.6 V. The oxidation peak at this potential suggests the formation of C = O bond-containing functional groups (carbonyl and carboxyl) within the rGO structure, while the reduction peak likely corresponds to the removal of these groups [33]. Notably, the presence of a weak and broad oxidation peak suggests a potentially hindered electron transfer, which might be due to the screening effect by the polymer matrix on the electroactive species. The areal capacitance value of 1.2 $\pm$ 0.4 mF cm^{-2} was calculated from CV data and is on par with the state-of-the-art rGO electrodes [34].

Our research then shifted to investigate the electron transfer characteristics of the rGO/PET electrodes. For this purpose, we took 5-mM potassium ferrocyanide (II) in 100-mM KCl as the supporting electrolyte. This molecule was chosen due to its well-documented one-electron redox reaction (1), commonly used as a benchmark in electrochemical studies

$$[Fe(CN)_6]^{4-} - \bar{e} \rightleftarrows [Fe(CN)_6]^{3-}. \quad (2)$$

CV conducted at a scan rate of 100 mV/s in the presence of $K_4[Fe(CN)_6]$ exhibited two pronounced redox peaks from the molecule, with an anodic peak at $E_A = 0.59$ V and a cathodic peak at $E_C = -0.13$ V, resulting in a peak separation value of $\Delta E = 0.72$ V [Fig. 2(b)]. We also investigated the influence of scan rate (diffusion layer thickness), ranging from 100 to 200 mV/s, on the CVs and peak current values. By plotting the peak current versus the square root of the scan rate [Fig. 2(c)], we assessed the charge transfer dynamics between the electrode and the electrolyte. The nearly perfect

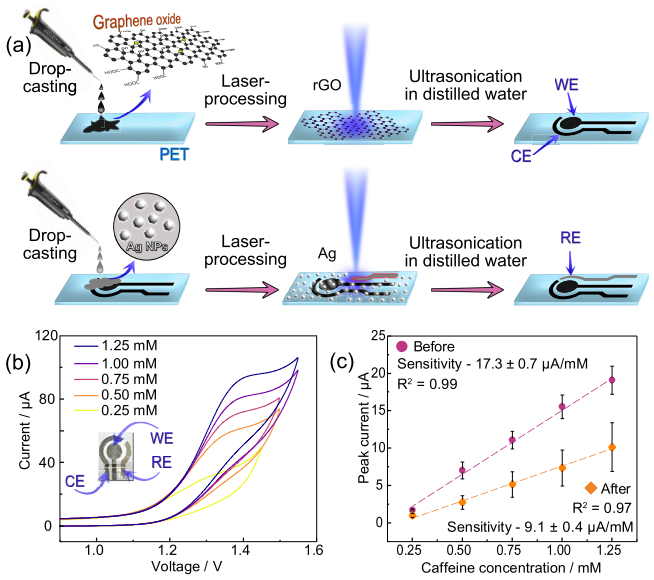

Fig. 3. (a) Schematic illustration of the "drop-sensor" fabrication. (b) CV curves recorded from the fabricated "drop sensor" in the presence of caffeine with different concentrations in BR buffer (pH 2). Inset is a picture of the "drop sensor." (c) Averaged calibration curve of the three sensors' current response versus caffeine concentration.

linear fit ($R^2 = 0.99$) indicates the fast charge transfer dynamics, unaffected by the polymer matrix or other external factors.

EIS is also a valuable tool for elucidating electron transfer processes. The Nyquist plot, particularly the high-frequency region typically represented by a semicircular shape, was analyzed to determine the charge transfer resistance (R_{ct}). In our case, R_{ct} was determined to be 264 Ω, providing valuable information about the electron transfer dynamics of the rGO/PET electrode system [Fig. 2(d)].

C. All Laser-Made "Drop Sensor"

We developed a fully laser-made sensor by capitalizing on the excellent electron transfer capabilities of the rGO/PET electrodes and leveraging our previous findings on the laser-driven integration of AgNPs into PET [35]. The synthesis exploits photothermal transduction from laser processing to melt the PET locally and sinter the AgNPs, embedding them partially within the PET yet ensuring exposure for sensor functionality, as described in earlier studies [34]. The production began with the assembly of rGO/PET composites as the base for the working and counter electrodes. Afterward, we applied a film of AgNPs to the cleared PET surface, which was then precisely laser-processed to create the silver reference electrode, as detailed in Fig. 3(a).

We tested the "drop sensor" with analytes to demonstrate its universal applicability in electrochemical sensing. Caffeine detection was performed using CV in the concentration range of 0.25–1.25 mM [Fig. 3(b)], typical in various beverages. The CV curves, in Britton–Robinson buffer (pH 2.1) as a supporting electrolyte, showed a caffeine oxidation peak to its 4,5-diol uric acid analog ($4\bar{e}$, $4H^+$ process) at $E = 1.35$ V, consistent with reports [36], [37]. Note that Fig. 3(b) focuses on the peak region of the CV curves, with the full range shown in Fig. S4. Comprehensive CV measure is critical in the whole range from −1.2 to 1.55 V to avoid compromising molecular signals due to adsorption, with negative voltage in CVs facilitating the desorption of adsorbed molecules. The sensor's current response exhibited a linear correlation with concentration ($R^2 = 0.98$), yielding a sensitivity of 17 ± 3 μA mM^{-1} and an estimated LoD of ca. 0.01 mM [Fig. 3(c)].

To evaluate the robustness of our flexible "drop sensors" created via laser processing, we conducted a series of bending tests to assess the impact on their sensing capabilities. Specifically, we investigated how the electrodes' performance would be affected after undergoing 1000 bending cycles at an angle of 165° (three-point bending setup shown in Fig. S4). This involved conducting CV measurements for the same caffeine concentration range before and after the bending process and then comparing the sensitivity.

The CV curves recorded before and after the bending cycles, consistently exhibited distinguishable caffeine oxidation peaks at $E = 1.35$ V (Figs. S4 and S6). The analysis of the peak current versus concentration plot revealed that the sensor's sensitivity after 1000 bending cycles was 9 ± 5 μA/mM [Fig. 3(c)], representing a modest reduction of less than ∼45% from the prebending sensitivity. Although the deviation might seem substantial, it is crucial to emphasize that this variance arises from averaging the data across three sensors. Individually, none of the sensors exhibited a decrease in sensitivity greater than 15%, indicating robust stability against mechanical deformations. Such a minimal deviation is acceptable for devices of this nature. The LoD for the sensor after bending was estimated to be 0.17 mM. Despite the slight changes in sensitivity and LoD, it is important to highlight that the bending process did not induce any significant structural changes in the electrodes. As a result, their performance remained largely consistent highlighting the durability and reliability of our full-laser-processed drop sensors.

To validate the real-world applicability of our sensor, we performed a blind test to detect an analyte concentration not previously evaluated. We prepared a caffeine solution at a 0.6-mM concentration and measured the sensor's response. When we added this new data point to the calibration curve—previously established after subjecting the sensor to 1000 bending cycles—it aligned seamlessly (as indicated by the red question mark in Fig. S7). This concordance confirms our sensor's effectiveness in determining unknown concentrations in practical scenarios.

Motivated by the exceptional performance of our sensor, we extended our investigation to include caffeine analysis in a real-world sample, demonstrating its practical applicability and selectivity. We purchased instant coffee from a local store and prepared a solution to quantify the caffeine content in 1 g of instant coffee. CV measurements of this solution, conducted with a BR buffer (pH 2) as the supporting electrolyte, allowed us to isolate the peak current value attributable to caffeine (Fig. S8). Using the calibration curve specific to this sample, we calculated the caffeine concentration in the solution, revealing that instant coffee contains approximately 30.6 ± 1.5 mg of caffeine per gram. To validate this finding, we conducted HPLC analysis on the same coffee

sample (Fig. S9), which indicated a caffeine concentration of about 36.7 mg g^{-1}, showing a ∼17% variance from our sensor's results. This discrepancy could arise from differences in sample preparation for EC and HPLC analyses—particularly, the incomplete dissolution of coffee in the EC method—resulting in a lower detected caffeine amount. Additionally, the nonuniform caffeine distribution in instant coffee may contribute to this difference. These insights confirm that our sensor can selectively detect caffeine amid other compounds, showcasing its potential for real-life applications.

Additionally, we investigated the "drop-sensor" versatility by testing its efficacy in glucose detection, another critical point-of-care analyte. The "drop sensor" exhibited behavior consistent with previous reports for glucose detection in KOH through CV [38]. The CV showed a clear and distinguishable oxidation peak at around 0.8 V, originating from the glucose oxidation to gluconic acid [39], [40]. Glucose sensing across a range of 1–35 mM (Fig. S10), a concentration window relevant to real-world applications, such as since, for blood glucose levels which typically vary between 2 and 40 mM [41]. Notably, at the higher concentration of 35 mM, the oxidation peak appeared to split into two, suggesting the possible formation of gluconolactone as an intermediate product in the reaction.

IV. Conclusion

We demonstrated the fabrication of a unique, flexible electrochemical "drop sensor" using a fully laser-integrated approach. By employing a multistep laser processing technique on various nanomaterial films deposited on PET, we successfully fabricated a "drop sensor" comprised of dual carbon electrodes (working and counter) and a silver electrode (reference). This sensor demonstrated its versatility in detecting critical point-of-care analytes, as exemplified by its capacity to accurately sense both glucose and caffeine within health-relevant concentration ranges.

A critical characteristic of our laser-induced composite formation is its ability to maintain the intrinsic structural integrity and mechanical properties of the substrate, thereby endowing the sensors with remarkable flexibility. This flexibility was crucial in our experiments and also a key novelty point of this work, where we were able to detect caffeine effectively before and after subjecting the sensors to 1000 bending cycles, without observing any significant degradation in their sensing performance. Such unique resilience highlights the practical potential of our "drop sensors" in various applications, where durability and adaptability are essential. Future research could explore the expansion of this technology, particularly due to the free-form nature of this method, to design comprehensive multianalyte monitoring systems capable of detecting a broader range of analytes.

References

[1] J. Wu, H. Liu, W. Chen, B. Ma, and H. Ju, "Device integration of electrochemical biosensors," *Nature Rev. Bioengineering*, vol. 1, no. 5, pp. 346–360, Feb. 2023.

[2] K. Wang, X. Lin, M. Zhang, Y. Li, C. Luo, and J. Wu, "Review of electrochemical biosensors for food safety detection," *Biosensors*, vol. 12, no. 11, p. 959, Nov. 2022, doi: 10.3390/bios12110959.

[3] Q. He et al., "Research on the construction of portable electrochemical sensors for environmental compounds quality monitoring," *Mater. Today Adv.*, vol. 17, Mar. 2023, Art. no. 100340.

[4] A. T. Lawal, "Progress in utilisation of graphene for electrochemical biosensors," *Biosensors Bioelectron.*, vol. 106, pp. 149–178, May 2018.

[5] S. J. Rowley-Neale, E. P. Randviir, A. S. Abo Dena, and C. E. Banks, "An overview of recent applications of reduced graphene oxide as a basis of electroanalytical sensing platforms," *Appl. Mater. Today*, vol. 10, pp. 218–226, Mar. 2018.

[6] J. Zhu et al., "Laser-induced graphene non-enzymatic glucose sensors for on-body measurements," *Biosensors Bioelectron.*, vol. 193, Dec. 2021, Art. no. 113606.

[7] S. Wang, Y. Liu, A. Zhu, and Y. Tian, "In vivo electrochemical biosensors: Recent advances in molecular design, electrode materials, and electrochemical devices," *Anal. Chem.*, vol. 95, no. 1, pp. 388–406, Jan. 2023.

[8] H. Yu et al., "Reduced graphene oxide nanocomposite based electrochemical biosensors for monitoring foodborne pathogenic bacteria: A review," *Food Control*, vol. 127, Sep. 2021, Art. no. 108117.

[9] H. Shamkhalichenar and J.-W. Choi, "Review—Non-Enzymatic hydrogen peroxide electrochemical sensors based on reduced graphene oxide," *J. Electrochemical Soc.*, vol. 167, no. 3, Jan. 2020, Art. no. 037531.

[10] Z. Wan, N.-T. Nguyen, Y. Gao, and Q. Li, "Laser induced graphene for biosensors," *Sustain. Mater. Technol.*, vol. 25, Sep. 2020, Art. no. e00205.

[11] L. Liu et al., "Electrochemically reduced graphene oxide-based electrochemical sensor for the sensitive determination of ferulic acid in A. Sinensis and biological samples," *Mater. Sci. Eng., C*, vol. 42, pp. 227–233, Sep. 2014.

[12] X. Zhang, Y.-C. Zhang, and J.-W. Zhang, "A highly selective electrochemical sensor for chloramphenicol based on three-dimensional reduced graphene oxide architectures," *Talanta*, vol. 161, pp. 567–573, Dec. 2016.

[13] M. A. Deshmukh, B.-C. Kang, and T.-J. Ha, "Non-enzymatic electrochemical glucose sensors based on polyaniline/reduced-graphene-oxide nanocomposites functionalized with silver nanoparticles," *J. Mater. Chem. C*, vol. 8, no. 15, pp. 5112–5123, 2020.

[14] H. Zhang and S. Liu, "Electrochemical sensors based on nitrogen-doped reduced graphene oxide for the simultaneous detection of ascorbic acid, dopamine and uric acid," *J. Alloys Compounds*, vol. 842, Nov. 2020, Art. no. 155873.

[15] Y. Zhang et al., "A flexible non-enzymatic glucose sensor based on copper nanoparticles anchored on laser-induced graphene," *Carbon*, vol. 156, pp. 506–513, Jan. 2020.

[16] H. S. M. Abd-Rabboh, A. E.-G. E. Amr, A. A. Almehizia, A. M. Naglah, and A. H. Kamel, "New potentiometric screen-printed platforms modified with reduced graphene oxide and based on man-made imprinted receptors for caffeine assessment," *Polymers*, vol. 14, no. 10, p. 1942, May 2022, doi: 10.3390/polym14101942.

[17] S. Yu, H. Li, G. Li, L. Niu, W. Liu, and X. Di, "Reduced graphene oxide-supported gold dendrite for electrochemical sensing of acetaminophen," *Talanta*, vol. 184, pp. 244–250, Jul. 2018.

[18] V. Suvina, S. M. Krishna, D. H. Nagaraju, J. S. Melo, and R. G. Balakrishna, "Polypyrrole-reduced graphene oxide nanocomposite hydrogels: A promising electrode material for the simultaneous detection of multiple heavy metal ions," *Mater. Lett.*, vol. 232, pp. 209–212, Dec. 2018.

[19] Y. Zhou et al., "Highly sensitive nitrite sensor based on AuNPs/RGO nanocomposites modified graphene electrochemical transistors," *Biosensors Bioelectron.*, vol. 146, Dec. 2019, Art. no. 111751.

[20] J. Baranwal, B. Barse, G. Gatto, G. Broncova, and A. Kumar, "Electrochemical sensors and their applications: A review," *Chemosensors*, vol. 10, no. 9, p. 363, 2022.

[21] G. Grosso, J. Godos, F. Galvano, and E. L. Giovannucci, "Coffee, caffeine, and health outcomes: An umbrella review," *Annu. Rev. Nutrition*, vol. 37, no. 1, pp. 131–156, Aug. 2017.

[22] D. Turnbull, J. V. Rodricks, G. F. Mariano, and F. Chowdhury, "Caffeine and cardiovascular health," *Regulatory Toxicology Pharmacol.*, vol. 89, pp. 165–185, Oct. 2017.

[23] Y. Guo, C. Zhang, Y. Chen, and Z. Nie, "Research progress on the preparation and applications of laser-induced graphene technology," *Nanomaterials*, vol. 12, no. 14, p. 2336, Jul. 2022, doi: 10.3390/nano12142336.

[24] P. Joshi, S. Shukla, S. Gupta, P. R. Riley, J. Narayan, and R. Narayan, "Excimer laser patterned holey graphene oxide films for nonenzymatic electrochemical sensing," *ACS Appl. Mater. Interface*, vol. 14, no. 32, pp. 37149–37160, Aug. 2022.

[25] R. K. Singh, P. S. Kumar, K. Amreen, S. K. Dubey, and S. Goel, "Disposable miniaturized electrochemical sensing platform with laser-induced reduced graphene oxide electrodes for multiplexed biochemical analysis," *IEEE Trans. Nanobiosci.*, vol. 22, no. 3, pp. 548–553, Jul. 2023.

[26] G. Yang, "Caffeine electrochemical sensor constructed by graphene oxide and reduced graphene oxide: A mini-review," *Current Anal. Chem.*, vol. 19, no. 6, pp. 448–456, Jul. 2023.

[27] I. Miccoli, F. Edler, H. Pfnür, and C. Tegenkamp, "The 100th anniversary of the four-point probe technique: The role of probe geometries in isotropic and anisotropic systems," *J. Phys., Condens. Matter*, vol. 27, no. 22, Jun. 2015, Art. no. 223201.

[28] A. Lipovka et al., "Textile electronics with laser-induced graphene/polymer hybrid fibers," *ACS Appl. Mater. Interface*, vol. 15, no. 32, pp. 38946–38955, Aug. 2023.

[29] D. Kogolev et al., "Waste PET upcycling to conductive carbon-based composite through laser-assisted carbonization of UiO-66," *J. Mater. Chem. A*, vol. 11, no. 3, pp. 1108–1115, 2023.

[30] R. D. Rodriguez et al., "Laser-engineered multifunctional graphene–glass electronics," *Adv. Mater.*, vol. 34, no. 43, Oct. 2022, Art. no. e2206877.

[31] A. Lipovka et al., "Photoinduced flexible graphene/polymer nanocomposites: Design, formation mechanism, and properties engineering," *Carbon*, vol. 194, pp. 154–161, Jul. 2022.

[32] R. D. Rodriguez et al., "Ultra-robust flexible electronics by laser-driven polymer-nanomaterials integration," *Adv. Funct. Mater.*, vol. 31, no. 17, p. 2008818, Apr. 2021.

[33] A. Y. S. Eng, A. Ambrosi, C. K. Chua, F. Šaněk, Z. Sofer, and M. Pumera, "Unusual inherent electrochemistry of graphene oxides prepared using permanganate oxidants," *Chem. A Eur. J.*, vol. 19, no. 38, pp. 12673–12683, Sep. 2013.

[34] Z. Wan, X. Chen, and M. Gu, "Laser scribed graphene for supercapacitors," *Opto-Electron. Adv.*, vol. 4, no. 7, 2021, Art. no. 200079.

[35] M. Fatkullin et al., "Molecular plasmonic silver forests for the photocatalytic-driven sensing platforms," *Nanomaterials*, vol. 13, no. 5, p. 923, Mar. 2023, doi: 10.3390/nano13050923.

[36] J.-Y. Sun, K.-J. Huang, S.-Y. Wei, Z.-W. Wu, and F.-P. Ren, "A graphene-based electrochemical sensor for sensitive determination of caffeine," *Colloids Surf. B, Biointerfaces*, vol. 84, no. 2, pp. 421–426, Jun. 2011.

[37] A. Carolina Torres, M. M. Barsan, and C. M. A. Brett, "Simple electrochemical sensor for caffeine based on carbon and nafion-modified carbon electrodes," *Food Chem.*, vol. 149, pp. 215–220, Apr. 2014.

[38] T. Jufík, P. Podešva, Z. Farka, D. Kovál, P. Skládal, and F. Foret, "Nanostructured gold deposited in gelatin template applied for electrochemical assay of glucose in serum," *Electrochimica Acta*, vol. 188, pp. 277–285, Jan. 2016.

[39] D. W. Hwang, S. Lee, M. Seo, and T. D. Chung, "Recent advances in electrochemical non-enzymatic glucose sensors—A review," *Anal. Chim. Acta*, vol. 1033, pp. 1–34, Nov. 2018.

[40] P. Gupta, V. K. Gupta, A. Huseinov, C. E. Rahm, K. Gazica, and N. T. Alvarez, "Highly sensitive non-enzymatic glucose sensor based on carbon nanotube microelectrode set," *Sens. Actuators B, Chem.*, vol. 348, Dec. 2021, Art. no. 130688.

[41] H. Lee, Y. J. Hong, S. Baik, T. Hyeon, and D. Kim, "Enzyme-based glucose sensor: From invasive to wearable device," *Adv. Healthcare Mater.*, vol. 7, no. 8, Apr. 2018, Art. no. 1701150.